Atmos. Chem. Phys. Discuss., 13, 13721–13772, 2013
www.atmos-chem-phys-discuss.net/13/13721/2013/
doi:10.5194/acpd-13-13721-2013

Atmospheric Chemistry and Physics Discussions

Comparison of mixed layer heights from airborne high spectral resolution lidar, ground-based measurements, and the WRF-Chem model during CalNex and CARES

A. J. Scarino[1], M. D. Obland[2], J. D. Fast[3], S. P. Burton[2], R. A. Ferrare[2], C. A. Hostetler[2], L. K. Berg[3], B. Lefer[4], C. Haman[5], J. W. Hair[2], R. R. Rogers[2], C. Butler[1], A. L. Cook[2], and D. B. Harper[2]

[1]Science Systems and Applications Inc., Hampton, Virginia, USA
[2]NASA Langley Research Center, Hampton, Virginia, USA
[3]Pacific Northwest National Laboratory, Richland, Washington, USA
[4]University of Houston, Dept. of Earth and Atmospheric Sciences, Houston, Texas, USA
[5]Trinity Consultants, Baton Rouge, Louisiana, USA

Received: 21 March 2013 – Accepted: 2 May 2013 – Published: 23 May 2013

Correspondence to: A. J. Scarino (amy.jo.scarino@nasa.gov)

Published by Copernicus Publications on behalf of the European Geosciences Union.

Abstract

The California Research at the Nexus of Air Quality and Climate Change (CalNex) and Carbonaceous Aerosol and Radiative Effects Study (CARES) field campaigns during May and June 2010 provided a data set appropriate for studying characteristics of the planetary boundary layer (PBL). The NASA Langley Research Center (LaRC) airborne High Spectral Resolution Lidar (HSRL) was deployed to California onboard the NASA LaRC B-200 aircraft to aid in characterizing aerosol properties during these two field campaigns. Measurements of aerosol extinction (532 nm), backscatter (532 and 1064 nm), and depolarization (532 and 1064 nm) profiles during 31 flights, many in coordination with other research aircraft and ground sites, constitute a diverse data set for use in characterizing the spatial and temporal distribution of aerosols, as well as the depth and variability of the daytime mixed layer (ML), which is a subset within the PBL. This work illustrates the temporal and spatial variability of the ML in the vicinity of Los Angeles and Sacramento, CA. ML heights derived from HSRL measurements are compared to PBL heights derived from radiosonde profiles, ML heights measured from ceilometers, and simulated PBL heights from the Weather Research and Forecasting Chemistry (WRF-Chem) community model. Comparisons between the HSRL ML heights and the radiosonde profiles in Sacramento result in a correlation coefficient value (R) of 0.93 (root-mean-square (RMS) difference of 157 m and bias difference (HSRL – radiosonde) of 57 m). HSRL ML heights compare well with those from the ceilometer in the LA Basin with an R of 0.89 (RMS difference of 108 m and bias difference (HSRL – Ceilometer) of −9.7 m) for distances of up to 30 km between the B-200 flight track and the ceilometer site. Simulated PBL heights from WRF-Chem were compared with those obtained from all flights for each campaign, producing an R of 0.58 (RMS difference of 604 m and a bias difference (WRF-Chem – HSRL) of −157 m) for CalNex and 0.59 (RMS difference of 689 m and a bias difference (WRF-Chem – HSRL) of 220 m) for CARES. Aerosol backscatter simulations are also available from

ACPD
13, 13721–13772, 2013

WRF-Chem and are compared to those from HSRL to examine differences among the methods used to derive ML heights.

1 Introduction

Since the mid 1960s, scientists have been researching different methods in order to determine the height of the planetary boundary layer (PBL) within the troposphere (Hosler and Lemmons, 1972; Stull, 1988; Heffter, 1980). The PBL can be further divided into discreet layers. For example, the daytime mixed layer (ML), also known as the convective boundary layer (CBL), is a subset of the PBL in which convectively driven eddies mix thermodynamic conditions, resulting in roughly uniform vertical profiles of moisture and potential temperature within that layer (Stull, 1988). The Division of Meteorology of the Environmental Protection Agency (EPA) indicated in 1965 the feasibility of remotely measuring vertical temperature profiles within the PBL (Hosler and Lemmons, 1972). During this feasibility study, a radiometer was developed and tested and provided adequate details in determining the height of the ML. A study in San Diego conducted in late 1971 and early 1972 (Noonkester et al., 1974) assessed the similarities and differences in lidar and high-resolution microwave radar echoes in measuring parameters within the PBL. In the 1981 NASA Goddard Space Flight Center report, Atlas and Korb (1981) examined the potential for using lidar observations for researching weather and climate. A portion of the report presents the use of aerosol profile measurements for determining PBL heights and utilizing this data in regional and global forecasting models through incorporation of the PBL height as a prognostic variable.

Even recently, in a 2009 report from the National Academy of Science (National Research Council, 2009), researchers are still recommending that determining the height of the atmospheric boundary layer is one of the highest priorities. There is also interest in ML height research for incorporation into weather and air quality forecasting models and for climate studies. The Department of Energy's Atmospheric System Research program includes in its science plan (Department of Energy, 2010) the importance

ACPD
13, 13721–13772, 2013

of measuring and studying ML heights by analyzing aerosol and cloud interactions, topographic features and tropospheric dynamics, which would be included in the development and evaluation of forecasting models.

Knowing the key parameters that are used to determine the ML height has been important as input to weather forecasting models. Utilizing PBL heights derived from radiosondes and ML heights from lidars to validate model forecasts will be useful for improvement of current models and formulation of future models. Several studies have been completed that examine how well various models perform when compared with ML heights derived from a radiosonde or a lidar. Angevine and Mitchell (2001) evaluated the National Centers for Environmental Prediction (NCEP) Mesocale Eta model using select radiosonde profiles during the summer months of 1997 and 1998 at the University of Illinois Bondville Road field site near Champaign-Urbana and again during the summer months of 1999 at the Cornelia Fort site in Nashville, Tennessee. The authors concluded that during the hours between 14:00 and 23:00 UTC (08:00 and 17:00 Central Standard Time), the Eta model is reasonably accurate (correlation coefficients (R) ranged from 0.75 to 0.82) compared to those heights derived from the radiosonde. During two of the three years, the comparisons were worse in the afternoon hours due to the prevalent cumulus cloud cover. Morning correlation coefficients (R) were $\sim$ 0.75 and were as low as 0.26 and 0.5 during the afternoon. A ground-based lidar was used to measure aerosol backscatter and estimate ML heights in the urban city of Zanjan, Iran. The lidar-estimated ML heights were compared to the ML heights estimated from the Fifth-Generation Mesoscale Model (MM5) forecast model (Bidokhti et al., 2008). Additionally, lidars on satellites have been utilized to evaluate models on a global scale. Measurements from the Cloud-Aerosol Lidar with Orthogonal Polarization (CALIOP) on the Cloud-Aerosol Lidar and Infrared Pathfinder Satellite Observations (CALIPSO) satellite are used to validate the Goddard Earth Observing System-version 5 (GEOS-5) Modern-Era Retrospective analysis for Research and Applications (MERRA) ML heights (Jordan et al., 2010). Extensive comparisons between the model output and the satellite observations in the Western Hemisphere and over

ACPD
13, 13721–13772, 2013

Africa resulted in correlation coefficients (R) ranging from 0.47 to 0.73. Furthermore, this study provided insight to regional ML height variances that might not be detected by a global circulation model. PBL heights from the global European Centre for Medium-Range Weather Forecasts (ECMWF) model were evaluated using ML heights derived from the Geoscience Laser Altimeter System (GLAS) (Palm et al., 2005). The ECMWF PBL heights were generally lower than the GLAS-derived ML height over the ocean, but small-scale and global patterns of ML heights revealed similar features.

Several field campaigns have been conducted and include comparisons of ML heights. The Atmospheric Mass Balance of Industrially Emitted and Natural Sulfur (AMBIENS) experiment in October 1977 estimated ML heights with sodar, lidar, and temperature profiles from a double theodolite balloon-tracking system (Coulter, 1979). During the 1992 Atlanta field intensive (Marsik et al., 1995), a combination of lidar, radiosonde, and wind profiler measurements were used to derive the ML heights, and a comparison was made between all three methods and results. The Pacific 1993 field campaign (Hayden et al., 1997) analyzed the vertical, chemical, and meteorological structure of the ML height in the lower Fraser Valley near Vancouver, Canada. This study utilized aircraft lidar, in situ instruments, and radiosondes to derive the ML heights. In early 2000, ground-based European Aerosol Research LIdar NETwork (EARLINET) and radiosondes were used to detect the seasonal evolution of the ML height (De Tomasi and Perrone, 2006) near Lecce, Italy for a period of two years. Since Lecce is located on a peninsula, the study also analyzed the effects of the sea breeze on the ML height. In general, these previous studies have demonstrated the ability to compute ML and PBL heights from a variety of instruments and methods. However, the majority of these studies rely on measurements obtained at limited number of sites so that the spatial variability of the boundary produced by models cannot be fully evaluated. More recently, the NASA Langley Research Center (LaRC) airborne High Spectral Resolution Lidar (HSRL) has been used for airborne atmospheric science campaigns and provides a unique source of data needed to evaluate simulated spatial and temporal variability of the boundary layer.

ACPD
13, 13721–13772, 2013

This paper provides a study of ML heights derived from the airborne HSRL compared with radiosondes, a ceilometer, and simulations made by the WRF-Chem model during the 2010 CalNex and CARES campaigns in California. Section 2 contains information on the HSRL instrument and an overview of the methods used to calculate the ML heights and Sect. 3 summarizes the locations, instruments involved, and science questions that are addressed for the CalNex and CARES field campaigns. Section 4 is divided between the CalNex and CARES campaigns and summarizes the HSRL ML height values in comparison with the values derived from radiosondes, a ceilometer, and the WRF-Chem model. Lastly, in Sect. 5, the sources of discrepancies in the WRF-Chem model and an explanation of these differences between the HSRL and simulated ML values are discussed.

2 Overview of methods used to compute the mixed layer height

In the literature, there are several methods used to define PBL or ML heights. These methods depend on the type of instrument being used, which typically are radiosondes, tethered balloons, wind profilers, lidars, ceilometers, or sodars. Various parameters measured by these instruments have been used to derive these heights, such as potential temperature, relative humidity, aerosol backscatter, wind speed, radar measurements of scattering from insects, and Richardson number. Many methods search for an inversion within the potential temperature or relative humidity profile or a sharp gradient in aerosol backscatter. Seibert et al. (2000) reviewed and completed an intercomparison of various methods used to determine the ML. The analysis included methods that use parcel lifting and Richardson number and applied them to radiosonde profiles. They also examined wind profiler data. It was determined that there are discrepancies among the methods analyzed, such as the definitions used and recommended that additional research is still needed in determining the ML heights. Seidel et al. (2010) compared seven methods that determine the PBL heights from radiosonde and surface observations over a 10 yr period. Temperature, potential temperature, virtual

ACPD
13, 13721–13772, 2013

potential temperature, relative humidity, specific humidity, and refractivity profiles are used in six of the methods, along with using a surface-based temperature to find the top of the surface-based inversion. Among the methods, it was found that the parcel method yielded heights almost 1000 m lower (range of heights were 500 m to 2000 m and parcel method heights were between 500 m and 750 m) than the other methods and is variable in diurnal and seasonal comparisons. The relative humidity and potential temperature gradient methods consistently yielded higher ML heights, anywhere from 100 m to 1000 m, than the other methods. We are using the definition that a ML height is the height of layer of the CBL seen in a well-mixed daytime aerosol backscatter profile from a lidar or ceilometer and a PBL height is from a single radiosonde profile measuring potential temperature, with launches from one to possibly six times a day.

2.1 Radiosonde profiles and the potential temperature gradients method

PBL heights can be derived from radiosonde profiles by using a technique suggested by Heffter (1980). Potential temperature from the radiosonde profiles is analyzed through an automatic algorithm that finds the critical inversion (e.g. Hayden et al., 1997; Marsik et al., 1995; Hennemuth and Lammert, 2006; Seidel et al., 2010). Heffter (1980) developed the method that would determine the vertical extent of mixing in a boundary layer model. This method analyzes the potential temperature to locate the critical inversion using the criteria based on the lapse rate and the inversion strength. Using this method, the potential temperature lapse rate ($\Delta\theta/\Delta z$) must be greater than or equal to 0.005 K m^{-1}. The inversion strength analyzed is represented using the potential temperature difference at the top and base of the layer ($\theta_{top} - \theta_{base}$), and that value must be greater than or equal to 2 K. Several other authors have taken this method and modified the criteria values (Hayden et al., 1997; Della Monache et al., 2004) by using lapse rates and inversion strengths that are more suited for a specific region. In this study, we chose the values that Hayden et al. (1997) chose for his study in the Lower Fraser Valley near Vancouver, Canada during the Pacific '93 field campaign, since it dealt with complex terrain, mountain valley circulation, and westerly wind flow (Pottier

ACPD
13, 13721–13772, 2013

et al., 1997), which are similar to the conditions found in the radiosonde launch locations during the 2010 CARES campaign. The criteria values from Hayden to identify the critical inversion are the following

$$\frac{\Delta\theta}{\Delta z} \geq 0.002\ \mathrm{K\,m^{-1}}, \quad (1)$$

$$\theta_{\mathrm{top}} - \theta_{\mathrm{base}} \geq 1\ \mathrm{K}. \quad (2)$$

With an automated algorithm, using the criteria values in Eqs. (1) and (2) to determine the PBL height from a potential temperature profile, the height is typically placed around where one would see the critical inversion. Figure 1 shows the potential temperature profiles for radiosonde launches that took place during the CARES campaign that display PBL height for the criteria in the above equations.

2.2 HSRL backscatter profiles and the wavelet transform method

The HSRL has acquired extensive datasets of aerosol extinction at 532 nm, backscatter at 532 nm and 1064 nm, depolarization at 532 nm and 1064 nm and aerosol optical depth (AOD) at 532 nm (Hair et al., 2008; Rogers et al., 2009). The instrument has flown aboard the NASA LaRC King Air B-200 and UC-12 aircraft on 349 science flights collecting 1142.4 h of data during 21 field campaigns in North America since 2006. For this study, ML heights are derived for HSRL daytime measurements using an automated technique that utilizes a Haar wavelet transform with multiple wavelet dilations (Brooks, 2003) to identify the sharp gradients in aerosol backscatter profiles located at the top of the boundary layer. Brooks' (2003) technique is an improvement over previous studies using wavelets (Davis et al., 2000; Cohn and Angevine, 2000), which were effective where the vertical backscatter gradient is small everywhere except at the mixed layer top, but which can produce a bias in the ML height estimates when a gradient is present above or within the ML (Brooks, 2003). Brooks (2003) attempted to eliminate this problem by developing an alternative technique that uses multiple wavelet dilations instead of a single dilation, thereby establishing the upper and lower limits of the backscatter

ACPD
13, 13721–13772, 2013

transition zone and identifying the altitude of the maximum of the aerosol gradient in the wavelet transform. This technique was found to be robust even in the presence of vertical gradients in the background signal. Brooks (2003) demonstrated this procedure using airborne backscatter lidar data acquired over relatively shallow marine boundary layers. In more varied meteorological conditions and over terrain, the mixed layer height can be more difficult to identify due to multiple sharp gradients in the profile that can correspond to aerosol layers lofted above the boundary layer or greater variability of aerosol within the boundary layer. Accordingly, the present authors have modified Brooks' (2003) technique to identify the lowest, not the strongest, significant aerosol gradient, as detailed in the following paragraphs. We have used the modified Brook's technique routinely across fifteen flight campaigns (212 flights, 729 h) and have found that it works reasonably well under a variety of meteorological and terrain conditions.

In this study, aerosol backscatter profiles (532 nm) derived from the HSRL measurements are the input data for the wavelet algorithm. These profiles are computed every 0.5 s using a 10 s running average of the HSRL 532 nm backscatter data (Hair et al., 2008). The aerosol backscatter values are averaged over ~ 1000 m horizontal and 30 m vertical resolution (Rogers et al., 2009). Clouds were removed from the analyses because they can produce signal gradients that can be misinterpreted by the wavelet algorithm as the boundary layer top. Following Davis et al. (2000), the largest negative Haar wavelets are used to identify cloudy profiles in the lidar data, using a flight-by-flight adaptive threshold that separates the cloud gradients from the weaker aerosol gradients (Burton et al., 2010).

The averaged cloud-free backscatter profiles are then used in the wavelet transform algorithm based on the method described by Brooks (2003). This algorithm computes a wavelet transform at multiple dilations, i.e., spatial distances, to compute the lower (H_1) and upper (H_2) limits of the transition zone, as well as the altitude of the maximum of the wavelet transform (H_3). The relationship among the three altitudes and the lidar backscatter profile can be seen in more detail in Fig. 2, which shows a single HSRL aerosol backscatter profile acquired at 20:06:42 UTC (13:06:42 PDT) on 25 May 2010

ACPD
13, 13721–13772, 2013

during the CalNex campaign. Davis et al. (1997) indicated that the depth ($H_2 - H_1$) of this transition zone might be a better estimate of the entrainment zone depth than the area-averaged value usually defined. Note that Cohn and Angevine (2000) computed entrainment zone thickness as the distance between the 15th and 85th percentiles of the lidar-derived ML heights, H_3. Therefore, in addition to providing H_1, H_2, and H_3, this research also provides heights corresponding to these percentiles computed with one-minute averages for each of H_1, H_2, and H_3. Brooks (2003) indicated that H_1, the lower limit of the transition zone, represents the top of the well-mixed layer. Because, however, Davis et al. (2000) and Cohn and Angevine (2000) used H_3, the altitude of the maximum wavelet transform, to identify the ML height, this article follows the same convention.

Comparison of the initial algorithm results with the ML heights obtained from visual inspection revealed some limitations of the Brooks algorithm, which were addressed by subsequent modifications. First, the algorithm would, at times, identify boundaries associated with elevated aerosol layers as the ML top. Consequently, the altitude region over which the algorithm searches for ML heights is limited to between $H_1 - 500$ m and $H_2 + 500$ m, using H_1 and H_2 from the previous minute. This is also why this method gives less stable results in cloudy cases because the clouds interrupt the one-minute window. Because of the large changes in ML height between land and water, the results computed over water are not used as a limit on the results over land, and vice versa. This restriction eliminates many of the false ML height detections.

Another modification was made to the algorithm to reduce the false detections owed to elevated aerosol layers as well as noise in the lidar signal. Therefore, the algorithm was modified to look for local maxima greater than an empirically determined threshold value, and choose the one at the lowest altitude. Examination of the heights from several flights shows these modification-produced results much closer to heights obtained by visual inspection.

An additional modification was made in the choice of dilation values used by the algorithm. The algorithm is designed to start with a small dilation that is on the order

ACPD
13, 13721–13772, 2013

of the vertical data resolution ($a_1 \approx 60$ m), which is then iteratively increased in size until the transition zone limits, H_1 and H_2, as well as the altitude of maximum in the wavelet transform, H_3, are found. Although this method provides good estimates of the transition zone limits, it often does not provide accurate estimates of H_3. The final "optimal" value of the dilation, a_2, which typically is about 200–300 m, is seemingly too small to accurately capture the location of the maximum in the wavelet transform. Consequently, the algorithm is adjusted to use a third, larger dilation value, a_3, for determining H_3. This larger dilation value is set to 900 m over land and 360 m over water. Thus, the optimal value of the dilation used to find H_3 appears to be a function of the boundary layer height. The smaller values of the optimal dilation found by Brooks (2003) are likely due to the much shallower marine ML heights that were examined in this earlier study. In contrast, higher mixed layers require larger dilation values. Figure 3 shows an example of the aerosol backscatter profiles for the 24 May 2010 flight over the Los Angeles basin. The deep purple lines represent one-minute running means of H_1 and H_2 and the white line represents a one-minute running mean of H_3. The ML top was easily identified by the algorithm as well as by visual inspection in the image.

Complicated aerosol structures within and/or above the ML, or clouds at the top of the ML, can prevent the algorithm from producing satisfactory results. Each flight is manually examined and a second set of ML heights is produced by visually inspecting the backscatter profiles. The heights produced by the automated algorithm are also considered part of this manual determination, thus this second set of "manual" heights is not independent of the set of heights determined from the automated method. The H_3 altitudes determined from the automated algorithm and the boundary layer heights determined from the manual inspection are combined to produce a set of "best estimate" boundary layer heights. In those cases where the H_3 altitudes from the automated algorithm and manual altitudes are within 300 m, the H_3 altitudes from the automated algorithm are used as the best estimate. If, however, the automated and manual altitudes differ by more than 300 m, the manual heights are used. Indeed, in many of the cases where the automated algorithm failed to give satisfactory results, it is also

ACPD
13, 13721–13772, 2013

difficult to accurately locate the ML height even by visual inspection. As an example of such a case, Fig. 4 shows the backscatter profiles for a portion of the flight near California's Central Valley on 18 June 2010. Note that the presence of aerosols above the ML between about 01:13 UTC and 01:19 UTC (which is displayed as 25.22 to 25.31 UTC on the plot) complicates the determination of ML height and causes the algorithm to incorrectly identify the ML height during this portion of this flight. The magenta line in the image shows the location of the "best estimate" ML height, which is obtained by combining the algorithm results with the ML height determined by visual inspection.

Figure 5 shows an example from a flight on 27 June 2010 during the CARES campaign. In this case, the ML height derived from the automated algorithm (shown by the white line in the left image) matches the height corresponding to gradients in the profiles of potential temperature and dew point as measured by a coincident radiosonde (shown by black dotted line in the right plot) launched just before 17:00 UTC (magenta dashed line, left plot). The lidar aerosol backscatter imagery on this date, however, shows that there can be significant aerosol above the ML height. The height of the maximum aerosol gradient (shown in purple) occurred well above the ML height in this case. Similarly, the radiosonde profiles show that the largest gradients in potential temperature and dew point (shown by purple dashed line) occurred above the ML height. For some applications, the full depth of the aerosol layer may be more relevant than the ML height. For this reason, the altitude of the maximum aerosol gradient has also been computed for all HSRL flights.

2.3 Ceilometer profiles and the aerosol backscatter gradients method

The aerosol backscatter retrievals from a ceilometer have also been utilized in determining the ML height. Ceilometers are limited to mostly cloud-free conditions because the laser pulse is attenuated when it hits dense clouds (Haman et al., 2012). The Vaisala ML height algorithm (version 3.5) was used to analyze the ceilometer backscatter coefficient to identify aerosol structures and determine the height of the ML using the negative gradient method (Münkel et al., 2007). The Vaisala ceilometer settings

ACPD
13, 13721–13772, 2013

during the CalNex campaign used a 5 % relative gradient to determine the threshold for a local gradient minimum to report where the ML height is located. The minimum height that the algorithm begins looking for a local gradient minimum is 30 m and then continues up to 2000 m, using the relative gradient threshold as an increment. Figure 6 shows an example of the ceilometer aerosol backscatter retrievals, along with the locations of the local gradient minimum. Height locations that the algorithm identifies as Local Minimum 1 are used as the ML height and the additional local gradient minimums reveal more information on boundary layer structures, such as residual layers or elevated aerosol layers (Münkel and Roinenen, 2008). However, inspection of the local minimum layers are done and it is possible that Local Minimum 2 and 3 could also be the location of the ML height. Additional information on the Vaisala ceilometer data used in this analysis can be found in Haman et al. (2012).

3 Field campaigns and data sets

3.1 CalNex – Los Angeles, CA – May 2010

The California Research at the Nexus of Air Quality and Climate Change (CalNex) campaign during May and June 2010 focused on air quality in the Los Angeles basin. In the CalNex Science White Paper (National Oceanic and Atmospheric Administration, 2008) there are several science questions that relate to the transport and meteorology of the basin. A few of the science questions refer to regional forecast models and include: Do regional models in California adequately represent these processes and their effect on air quality? What are proper oceanic boundary conditions for coastal and regional atmospheric chemistry modeling? What are the major deficiencies in the representation of chemistry and meteorology in research and operational models and how can models be improved through the collection of additional measurements? Having extensive data on the ML height is useful in answering these science questions since it defines the vertical extent of mixing (e.g. dilution) of trace gases and aerosols

ACPD
13, 13721–13772, 2013

in the boundary layer. In addition to ML height, knowledge of the airflow where the aerosols are located in areas of complex terrain is important in validating research and operational forecasting models, such as WRF-Chem. During CalNex, there were three aircraft outfitted with atmospheric measurement instruments, a research vessel also carrying atmospheric measurement instruments, and a suite of ground-based instruments (Ryerson et al., 2012). The aircraft included the NOAA Twin Otter, NOAA WP-3D, and the NASA King Air B-200, which was outfitted with the NASA LaRC High Spectral Resolution Lidar (HSRL). The suite of ground-based instruments located in Pasadena, CA (latitude: 34.14° N, longitude: 118.12° W, altitude: ~ 240 m m.s.l.) included instruments that measured atmospheric chemistry and aerosol parameters. Among those instruments was a Vaisala ceilometer, operated by a research group from the University of Houston (Haman et al., 2012). During the CalNex campaign, the NASA B-200 completed eight science flights during May 2010. Figure 7 shows ground tracks of the B-200 flights during CalNex.

The Los Angeles basin is bordered by the San Gabriel Mountains, the San Bernardino Mountains, and the Pacific Ocean. The basin is impacted by sea breezes and mountain flows that can transport or trap aerosols (Neuman et al., 2012). Duong et al. (2011) analyzed wind roses in the basin and found that the general wind patterns involved westerly and southwesterly winds transporting air from the Pacific Ocean border of the basin toward the mountainous regions and then funneling it through the narrow passes into the desert regions. Other studies have been completed in the Los Angeles basin to analyze the vertical distributions of the elevated polluted layers and the structure of the ML height. McElroy and Smith (1986 and 1991) looked at the vertical pollutant distributions and the ML structure with an airborne lidar in both 1982 and 1985. They found that the air transport in an area near a coastline and with a complex terrain greatly affects the varying ML heights and the location of pollutants within those layers. Lidar observations of polluted layers over Los Angeles during the Basic Studies on Airflow, Smog and the Inversion (BASIN) project in the summer of 1984 were the focus of a study by Wakimoto and McElroy (1986) using lidar observations of pol-

ACPD
13, 13721–13772, 2013

luted layers over Los Angeles. The BASIN study included a network of locations where radiosondes were launched every four hours and aircraft cross-sections showing vertical profiles of the atmosphere were made over these locations to have a rich dataset of lidar observations and the parameters from the radiosonde profiles. Wakimoto and McElroy (1986) concluded that upper-level winds, along with thermal changes along a complex terrain, control the evolution of the polluted layers within the depth of the ML.

3.2 CARES – Sacramento, CA – June 2010

The Carbonaceous Aerosol and Radiative Effects Study (CARES) took place in the Sacramento, CA region during June 2010. One of the objectives from this campaign is to study the Sacramento urban plume, how it transports throughout the region, and how it is mixed into the atmosphere (Zaveri et al., 2012). The CARES campaign used two primary aircraft, the DOE G-1 and the NASA King Air B-200. Since the CARES schedule overlapped with CalNex, the NOAA WP-3 and Twin Otter aircraft participated in some of the central California flights. There were also two ground sites utilized during CARES: the T0 site, located at American River College (latitude: 38.65° N, longitude: 121.35° W, altitude: 30 m m.s.l.) in Sacramento, and the T1 site, located at Northside School (latitude: 38.87° N, longitude: 121.02° W, altitude: 454 m m.s.l.) in Cool, CA, which is about 40 km northeast of Sacramento. Very comprehensive suites of instruments were located at these ground sites, measuring meteorological parameters, trace gases, optical properties of aerosols, aerosol composition, aerosol size distributions and solar radiation. Radiosondes were also launched from these ground sites about four times per day on the days with science flights to capture the evolution of the atmosphere. In total there were twenty-three science flights by the NASA B-200 during CARES. Figure 8 shows ground tracks of the B-200 flights during CARES, along with three regions discussed in Sect. 4.2.2 and the locations of the ground sites.

Fast et al. (2012) discusses the dominant meteorological conditions over central California encompassing Sacramento, San Francisco, and the Sierra Nevada mountains.

ACPD
13, 13721–13772, 2013

In general there was either a southwesterly or northwesterly near-surface winds in the central valley, along with down-slope and down-valley flows over the Sierra Nevada Mountains. Dillon et al. (2002) also examined the Sacramento urban plume during a summer 1997 study located on the western slope of the Sierra Nevada Mountains. Their work mentions that the main source of pollution in the Sacramento plume is vehicular traffic. This plume is controlled by extremely consistent, terrain-driven winds that bring the polluted air into the mountains during the day and then the polluted air is flushed out at night by a clean continental airflow that is reversed.

4 Comparison of mixed layer heights

4.1 LA Basin during CalNex

Output from the WRF-Chem model (Grell et al., 2005) was processed along the King Air B-200 flight tracks to produce direct spatial and temporal comparisons between the HSRL-derived ML heights and PBL heights computed from the model. The configuration of WRF-Chem for the CalNex and CARES campaigns is described in Fast et al. (2012). The model employed the Mellor-Yamada-Janjić (MYJ) (Janjić, 1990, 2002) parameterization scheme and the simulated boundary layer is determined where the vertical gradient in potential temperature exceeds a threshold. The boundary layer height and profiles of meteorological quantities were extracted at the closest model grid cell to each HSRL sampling location and interpolated linearly in time between hourly output intervals to the HSRL sampling times. The HSRL values used were the "best estimate" ML heights described in Sect. 2.2. WRF-Chem PBL and HSRL ML height (both heights are above ground level (AGL)) comparisons show reasonable agreement between model output and the airborne measurements across all flights during CalNex, as shown by the scatter and regression plot in Fig. 9. The region from which the data used in this scatter and regression plot were obtained is bounded by the 35° N line, as shown in Fig. 7, to include only the flights in the LA Basin. The regression

ACPD
13, 13721–13772, 2013

plot produces an R of 0.58 with a bisector slope of 0.87 and intercept of −8.6 m using over 106 000 data points. The bias difference between modeled PBL and measured ML heights (WRF-Chem – HSRL) is −157 m with the root-mean-square (RMS) difference being 604 m.

These same modeled and measured data are partitioned by time in Fig. 10 to show the diurnal pattern of the PBL and ML heights around the Los Angeles area in terms of percentiles for the flight hours over the entire CalNex campaign. The hourly median values between the two methods agree to within a few hundred meters throughout most of the day. The largest difference of about 700 m between hourly median values was found to be in the late afternoon after 15:00 LST.

Evaluations of ML heights at AGL from the ceilometer at the Pasadena, CA ground site and HSRL were performed to compare the two instruments' measurements against each other and to better understand the extent to which the ceilometer measurements of ML height were indicative of the ML height throughout the CalNex study area. HSRL data were screened to find the points of closest spatial approach between the B-200 aircraft and the Pasadena ground site, both within ±7.5 min of the times of a ceilometer measurement and within various linear separation ranges. Note that the ceilometer typically made a measurement every 15 min.

Regression scatter plots of the results, shown in Fig. 11, illustrate that the HSRL and ceilometer data agree very well up to a separation distance of about 30 km, with an R of 0.89 for the 18 comparison points and an RMS difference of 108 m and bias difference (HSRL – Ceilometer) of −9.7 m within that distance (left plot). The comparison breaks down quickly past 30 km, and produces an R of 0.08 and an RMS difference of 554 m and bias difference (HSRL – Ceilometer) of 234 m for points between 30 km and 50 km (right plot), and is essentially uncorrelated when including the 50 points of comparison between 50 km separation distance and the maximum separation distance during the entire study of approximately 310 km. This result is not unexpected, as beyond 30 km from the Pasadena ground site the B-200 flew over ocean and high altitude terrain and differences in surface characteristics and altitude can dramatically affect boundary

ACPD
13, 13721–13772, 2013

layer growth. If the comparison points are further limited to only consider points when the HSRL took data over ground altitudes that were within ±200 m of the altitude of the Pasadena ground site, the comparison improves and agreement can be found up to separation distances up to about 100 km. Up to 50 km, the R is 0.83 for 23 comparison points within that distance, from 50 km to 100 km, the R is 0.69 for 9 points, and from 100 km to 150 km, the R is 0.36 for 10 points.

The spread of all HSRL-derived ML heights encountered as the B-200 flew within ±7.5 min of each ceilometer measurement, though not limited by separation distance, is plotted as horizontal lines for each point of closest approach in Fig. 11. From inspection of these spreads, it is evident that while there is very good agreement between the ceilometer and HSRL when the two measurements are close in space and time, the ML height can vary by large amounts, up to as much as 1 km, in locations surrounding the ceilometer. This is likely due to variations of ML heights with the terrain, differing meteorological conditions over the ocean and mountains, and different air masses within the study region. Figure 12 shows the diurnal pattern of the ceilometer ML heights during CalNex and indicates that the ML only changed by approximately 100 m at most during a 15 min span, and thus the changes seen between the ceilometer and HSRL were not primarily functions of ML evolution.

Differences in the ML heights between the HSRL and ceilometer using portions of the flights from 19 and 20 May 2010, as examples, are plotted on a Google Earth image of the LA Basin in Fig. 13. The ceilometer ML heights were subtracted from the HSRL ML heights within up to ±15 min of the aircraft overpass and the data were limited to ground altitudes of 500 m or less (i.e., the LA basin). On 19 May (left image), the ceilometer data correlated closely with the ML heights throughout the region, whereas on 20 May (right plot), the ML heights did show differences up to 1000 m or more, even very close to the ceilometer site.

ACPD
13, 13721–13772, 2013

4.2 Sacramento region during CARES

4.2.1 Radiosonde profile and HSRL mixed layer heights

Since the T0 and T1 sites are located in the central valley and at the foothills of the Sierra Nevada Mountains, respectively, we conducted our analysis of these sites separately. Since radiosonde launches did not exactly correspond with the aircraft overpass times, we limited our comparison data to separation distance of 15 km and temporal difference of 30 min between the aircraft and the radiosondes. Figure 14 summarizes the comparisons of PBL and ML heights (both AGL). At the T0 site, the comparisons resulted in an R of 0.91, RMS difference of 140 m and a bias difference (HSRL – radiosonde) of −12 m. At the T1 site, the comparisons resulted in an R of 0.97, RMS difference of 174 m and a bias difference of 130 m. When the comparisons for the T0 and T1 sites are combined, it results in an R of 0.93, RMS difference of 157 m and a bias difference of 57 m.

4.2.2 WRF-Chem model and HSRL mixed layer heights

As with the CalNex flights, the WRF-Chem model was processed along the King Air B-200 flight tracks for CARES to produce direct spatial and temporal comparisons between the HSRL-derived ML heights and the PBL heights computed from the model. WRF-Chem settings for this comparison are the same used during CalNex and described in Sect. 4.1; however for the CARES campaign, the model settings were adjusted for the Sacramento region and only processed along the reduced HSRL dataset. The HSRL values used were the "best estimate" ML heights described in Sect. 2.2. WRF-Chem PBL and HSRL ML height comparisons show reasonable agreement between the model output and the airborne measurements across all flights during CARES, as shown by the scatter and regression density plot in Fig. 15. The regression plot produces an R of 0.59 with a bisector slope of 1.56 and intercept of −288 m using over 3200 data points. The bias difference between modeled PBL and measured ML

ACPD
13, 13721–13772, 2013

heights (WRF-Chem – HSRL) is 220 m, with the RMS difference being 689 m. These same modeled and measured data are partitioned by time in Fig. 16 to show the diurnal pattern of the PBL and ML heights in central California in terms of percentiles for the flight hours over the entire CARES campaign. The median values between the two methods agree to within a few hundred meters throughout most of the day. The largest difference of about 200 m between median values was found to be in the early morning between 08:00 and 09:00 LST.

Since the entire region that was studied during CARES has complex terrain, we divided it into three areas – San Francisco Bay, Central Valley (that includes Sacramento and the T0 ground site) and the Sierra Nevada (includes the T1 ground site) – for further analysis of the ML height values from both HSRL and WRF-Chem. Figure 8 shows how the regions are divided and the locations of the ground sites. Within the Central Valley region, the main focus area of the CARES campaign, just over 15 400 data points are available for comparison. WRF-Chem and HSRL ML height comparisons show reasonable agreement between model output and the airborne measurement across the flights within the Central Valley region, as shown by the scatter and regression plot in Fig. 17. The regression plot produces an R of 0.69 with a bisector slope of 1.50 and intercept of −307 m. The bias difference between modeled PBL and measured ML heights (WRF-Chem – HSRL) is 134 m with the RMS difference being 561 m. A poorer agreement between the model and airborne measurements was found for the Sierra Nevada and San Francisco regions. As shown in Fig. 18, the regression plot produces an R of 0.48 with a bisector slope of 1.53 and intercept of 82 m using over 7500 data points. The bias difference between modeled PBL and measured ML heights (WRF-Chem – HSRL) is 608 m with the RMS difference being 880 m. In contrast to the Sierra Nevada region, the simulated PBL in the San Francisco region is lower than those obtained from HSRL as shown in Fig. 19. The bias difference between modeled PBL and measured ML heights (WRF-Chem – HSRL) is −170 m with the RMS difference being 521 m. The regression plot produces an R of 0.41 with a bisector slope of 0.99 and intercept of −161 m using over 5900 data points.

ACPD
13, 13721–13772, 2013

While there was agreement in the comparisons between HSRL ML and WRF-Chem PBL heights for the entire CARES region, the ML and PBL heights are derived using two different methods – aerosol backscatter versus potential temperature. During the CARES campaign, the WRF-Chem model, along the HSRL flight tracks, also computed simulated aerosol backscatter profiles. The simulated backscatter was processed through the same wavelet covariance transform method used to produce the HSRL ML heights. Thus, deriving ML heights from WRF-Chem backscatter profiles provides a more direct comparison to the HSRL ML heights. The comparison of ML heights computed using WRF-Chem aerosol backscatter profiles shown in Fig. 20 is very similar to the comparison of PBL heights computed using the WRF-Chem potential temperatures shown in Fig. 15. The R for the WRF-Chem and HSRL ML height comparison shown in Fig. 20 is 0.60. There was only a small improvement in R between methods, showing that, at least in these cases, both methods yielded very similar results. The second research flight on 14 June 2010 is shown in Fig. 21 with the aerosol backscatter measured from HSRL with ML heights overlaid in white and simulated aerosol backscatter from WRF-Chem with PBL heights from potential temperature in black and ML heights from aerosol backscatter in white. A scatter density plot comparing HSRL aerosol backscatter and simulated WRF-Chem aerosol backscatter for this second research flight on 14 June is shown in Fig. 22. These plots demonstrate that although the WRF-Chem simulations of aerosol backscatter and PBL height are generally in good agreement with the HSRL measurements, the simulations sometimes have difficulty in accurately forecasting the vertical extent of aerosols in the ML as well as the magnitude of aerosol backscatter both in the boundary layer and the free troposphere. In addition to the treatment of atmospheric chemistry, particularly secondary organic aerosol, emissions of primary aerosols and aerosol precursors over California, and boundary conditions also effect predictions of aerosols that will be described in a subsequent study.

ACPD
13, 13721–13772, 2013

5 Summary

HSRL aerosol backscatter was used to derive ML heights and assess simulations of the temporal and spatial variability of PBL and ML heights in both the CalNex and CARES study regions. The ML height assessments are critical for evaluation of the performance of research forecasting models like WRF-Chem when they are used for air quality assessments.

In the diurnal variation plot analyzing HSRL ML heights and WRF-Chem PBL heights during CalNex, it showed the largest median difference was found in the late afternoon. One of the reasons for the differences is associated with the technique used in finding the ML and PBL height. It could also be associated with how boundary layer treatments in models perform over regions of complex terrain and variable surface properties, since portions of the flights during CalNex were over the San Bernardino and San Gabriel Mountains, and over both land and water. During CARES, the diurnal behavior of the differences between the HSRL ML and WRF-Chem PBL heights was different in that the largest difference was found to be in the early morning hours between 08:00 and 09:00 LST. While this difference was not as large as the CalNex median difference, it could be attributed to a residual layer of the previous days mixed layer that is identified in aerosol backscatter, but is not shown in a potential temperature profile.

To evaluate the impact of the complex terrain in the CARES study region, the domain was divided into the three regions to see how well the model simulations of PBL performed as a function of location. WRF-Chem performed best over the Central Valley with an R of 0.69 and this is most likely due to the flight being constrained to a region with a flat terrain. The complex terrain and bodies of water affected the WRF-Chem results over the Sierra Nevada and San Francisco regions, with an R of 0.48 and 0.41, respectively. Over the Sierra Nevada region, WRF-Chem PBL heights were higher than the HSRL ML heights, as shown in Fig. 18. Comparisons that took place over the San Francisco Bay, resulted in lower heights from both HSRL and WRF-Chem, however

ACPD
13, 13721–13772, 2013

Fig. 19 shows that there are a number of occurrences where the WRF-Chem PBL heights are much lower than the HSRL ML heights for this region.

Conducting the comparison of ML heights between HSRL and WRF-Chem did give insight regarding differences in PBL heights produced by different techniques (e.g. aerosol gradients vs. potential temperature gradients). When compared to the HSRL ML heights, there was very little, if any difference between WRF-Chem PBL computed using aerosol gradients and potential temperature gradients. This supports the use of the ML computed from aerosol backscatter gradients as a proxy for the PBL. This also suggests that other factors in the modeling and/or HSRL ML height retrieval techniques were responsible for differences between the HSRL and WRF-Chem PBL heights.

The HSRL ML heights during the CalNex campaign were compared with the corresponding ML heights computed from a ground-based ceilometer located in Pasadena, CA. Overall these heights agreed well (R is 0.89) when HSRL is within 30 km of the ceilometer. Within this range, variations in how the algorithms assign the ML height to the appropriate aerosol gradient may account for the differences in the ML heights between the ceilometer and HSRL. Haman et al. (2012) states in her paper that the ceilometer does a very good job detecting the aerosol layers, but the detection of the ML height becomes difficult immediately following a frontal system that brings precipitation and high winds to the location of the ceilometer. These conditions act to washout and prevent accumulation of the aerosols. Other problems with the ML height detection occur in the late afternoon and early evening hours when convection is weakening, the boundary layer is collapsing, and the aerosol layers aloft do not represent the true ML height.

The comparisons of the ML heights derived from HSRL and the PBL heights from radiosonde potential temperature profiles showed reasonable agreement. Caveats of this comparison are similar to that of WRF-Chem, that the comparisons of ML heights are derived differently. While the radiosonde derived ML heights compared well (R is 0.93) to the HSRL ML heights, possible reasons for the differences are associated with the many ways to compute PBL heights and these differences are due to the

ACPD
13, 13721–13772, 2013

techniques. While we selected a modified Heffter method for the inversion constraints, it is possible that other values could be considered depending on the time when the radiosonde is launched and other atmospheric parameters. Other methods, such as using relative humidity and wind speed to determine the ML height may be explored.

The results presented here demonstrate that the ML heights derived from HSRL aerosol backscatter profiles are closely comparable to those derived from radiosonde temperature profiles, and that these HSRL ML heights can be used to evaluate ML and PBL heights from other sensors (e.g. ceilometers) and models. The HSRL ML heights also provide additional information to modelers that are either updating or developing the parameterization schemes used in simulations of where the PBL is located.

In future studies, we will be analyzing the large data set from HSRL that has research flights from 21 field campaigns in North America from 2006 to 2012. The HSRL data collected during these campaigns have been used for computing ML heights and will be used to assess additional simulations of WRF-Chem, along with the NASA Goddard Earth Observing System – version 5 (GEOS-5), and European Centre for Medium-Range Weather Forecasts – Monitoring Atmospheric Composition and Climate (ECMWF-MACC).

Acknowledgements. The funding for this research came from the NASA Science Mission Directorate, the Department of Energy Atmospheric Systems Research program (Interagency Agreement DE-AI02-05ER63985), the Office of Science, Office of Biological and Environmental Research (OBER), and the NASA CALIPSO project. DOE's ARM Climate Research Facility supported logistics and data collection during CARES. We would also like to thank Dave Turner for writing a significant amount of the code for the Haar Wavelet Covariance program that is applied to the HSRL aerosol backscatter. The authors would also like to thank the NASA Langley King Air B-200 flight crew for their outstanding work supporting these flights and measurements.

References

Angevine, W. and Mitchell, K.: Evaluation of the NCEP mesoscale eta model convective boundary layer for air quality applications, Mon. Weather Rev., 129, 2761–2775, 2001.

ACPD
13, 13721–13772, 2013

Atlas, D. and Korb, C. L.: Weather and climate needs for lidar observations from space and concepts for their realization, B. Am. Meteorol. Soc., 62, 1270–1285, 1981.
Bidokhti, A. A., Khoshsima, M., Sabetghadam, S., and Khalesifard, H. M.: Estimation of urban mixed layer height in Zanjan using LIDAR observations and numerical modeling, J. Earth Syst. Sci., 117, 925–934, 2008.
Brooks, I. M.: Finding boundary layer top: Application of wavelet covariance transform to Lidar backscatter profiles, J. Atmos. Ocean. Tech., 20, 1092–1105, 2003.
Burton, S. P., Ferrare, R. A., Hostetler, C. A., Hair, J. W., Kittaka, C., Vaughan, M. A., Obland, M. D., Rogers, R. R., Cook, A. L., Harper, D. B., and Remer, L. A.: Using airborne high spectral resolution lidar data to evaluate combined active plus passive retrievals of aerosol extinction profiles, J. Geophys. Res.-Atmos., 115, D00H15, doi:10.1029/2009JD012130, 2010.
Cohn, S. and Angevine, W.: Boundary layer height and entrainment zone thickness measured by lidars and wind-profiling radars, J. Appl. Meteorol., 39, 1233–1247, 2000.
Coulter, R. L.: A comparison of three methods for measuring mixing-layer height, J. Appl. Meteorol., 18, 1495–1499, 1979.
Davis, K. J., Lenschow, D. H., Oncley, S. P., Kiemle, C., Ehret, G., and Giez, A.: The role of entrainment in surface-atmosphere interactions over the boreal forest, J. Geophys. Res.-Atmos., 102, 29219–29230, 1997.
Davis, K. J., Gamage, N., Hagelberg, C. R., Kiemle, C., Lenschow, D. H., and Sullivan, P. P.: An objective method for deriving atmospheric structure from airborne lidar observation, J. Atmos. Ocean Tech., 17, 1455–1468, 2000.
Delle Monache, L., Perry, K. D., Cederwall, R. T., and Ogren, J. A.: In situ aerosol profiles over the Southern Great Plains and cloud and radiation test bed site: 2. Effects of mixing height on aerosol properties, J. Geophys. Res.-Atmos., 109, D06209, doi:10.1029/2003JD004024, 2004.
Department of Energy Atmospheric System Research Science and Program Plan: http://science.energy.gov/~/media/ber/pdf/Atmospheric_system_research_science_plan.pdf, last access: 7 July 2012, 2010.
De Tomasi, F. and Perrone, M. R.: PBL and dust layer seasonal evolution by lidar and radiosounding measurements over a peninsula site, Atmos. Res., 80, 86–103, 2006.

ACPD
13, 13721–13772, 2013

Dillon, M. B., Lamanna, M. S., Schade, G. W., Goldstein, A. H., and Cohen, R. C.: Chemical evolution of the Sacramento urban plume: transport and oxidation, J. Geophys. Res.-Atmos., 107, 4046, doi:10.1029/2001JD000779, 2002.

Duong, H. T., Sorooshian, A., Craven, J. S., Hersey, S. P., Metcalf, A. R., Zhang, X., Weber, R. J., Jonsson, H., Flagan, R. C., and Seinfeld, J. H.: Water-soluble organic aerosol in the Los Angeles Basin and outflow regions: Airborne and ground measurements during the 2010 CalNex field campaign, J. Geophys. Res.-Atmos., 116, D00V04, doi:10.1029/2011JD016674, 2011.

Emeis, S., Schäfer, K., Münkel, C., Friedl, R., and Suppan, P.: Evaluation of the interpretation of ceilometer data with RASS and radiosonde data, Bound.-Lay. Meteorol., 143, 25–35, 2012.

Fast, J. D., Gustafson Jr., W. I., Berg, L. K., Shaw, W. J., Pekour, M., Shrivastava, M., Barnard, J. C., Ferrare, R. A., Hostetler, C. A., Hair, J. A., Erickson, M., Jobson, B. T., Flowers, B., Dubey, M. K., Springston, S., Pierce, R. B., Dolislager, L., Pederson, J., and Zaveri, R. A.: Transport and mixing patterns over Central California during the carbonaceous aerosol and radiative effects study (CARES), Atmos. Chem. Phys., 12, 1759–1783, doi:10.5194/acp-12-1759-2012, 2012.

Grell, G. A., Peckham, S. E., Schmitz, R., McKeen, S. A., Frost, G., Skamarock, W. C., and Eder, B.: Fully coupled "online" chemistry within the WRF model, Atmos. Environ., 39, 6957–6976, 2005.

Haeffelin, M., Angelini, F., Morille, Y., Martucci, G., Frey, S., Gobbi, G. P., Lolli, S., O'Dowd, C. D., Sauvage, L., Xueref-Rémy, I., Wastine, B., and Feist, D. G.: Evaluation of mixing-height retrievals from automatic profiling lidars and ceilometers in view of future integrated networks in Europe, Bound.-Lay. Meteorol., 143, 49–75, 2012.

Hair, J. W., Hostetler, C. A., Cook, A. L., Harper, D. B., Ferrare, R. A., Mack, T. L., Welch, W., Izquierdo, L. R., and Hovis, F. E.: Airborne high spectral resolution Lidar for profiling aerosol optical properties, Appl. Optics, 47, 6734–6752, doi:10.1364/AO.47.006734, 2008.

Haman, C., Lefer, B., and Morris, G.: Seasonal variability in the diurnal evolution of the boundary layer in a near coastal urban environment, J. Atmos. Ocean Tech., 29, 697–710, 2012.

Hayden, K. L., Anlauf, K. G., Hoff, R. M., Strapp, J. W., Bottenheim, J. W., Wiebe, H. A., Froude, F. A., Martin, J. B., Steyn, D. G., and McKendry, I. G.: The vertical chemical and meteorological structure of the boundary layer in the lower fraser valley during PACIFIC '93, Atmos. Environ., 31, 2089–2105, 1997.

ACPD
13, 13721–13772, 2013

Heffter, J. L.: Transport layer depth calculations, Second Joint Conference on Applications of Air Pollution Meteorology, New Orleans, LA, 24–27 March 1980, 12.11, 1980.
Hennemuth, B. and Lammert, A.: Determination of the atmospheric boundary layer height from radiosonde and lidar backscatter, Bound.-Lay. Meteorol.,120, 181–200, 2006.
Hosler, C. R. and Lemmons, T. J.: Radiometric measurements of temperature profiles in the planetary boundary layer, J. Appl. Meteorol., 11, 341–348, 1972.
Janjić, Z. I.: The step-mountain coordinate: physical package, Mon. Weather Rev., 118, 1429–1443, 1990.
Janjić, Z. I.: Nonsingular implementation of the Mellor-Yamada Level 2.5 scheme in the NCRP Meso model, NCEP Office Note 437, 61 pp., 2002.
Jordan, N. S., Hoff, R. M., and Bacmeister, J. T.: Validation of Goddard Earth Observing System-version 5 MERRA planetary boundary layer heights using CALIPSO, J. Geophys. Res., 115, D24218, doi:10.1029/2009JD013777, 2010.
Marsik, F. J., Fischer, K. W., McDonald, T. D., and Samson, P. J.: Comparison of methods for estimating mixing height used during the 1992 Atlanta Field Intensive, J. Appl. Meteorol., 34, 1802–1814, 1995.
McElroy, J. and Smith, T.: Vertical pollutant distributions and boundary layer structure observed by airborne lidar near the complex southern california coastline, Atmos. Environ., 20, 1555–1566, 1986.
McElroy, J. and Smith, T.: Lidar descriptions of mixing-layer thickness characteristics in a complex terrain/coastal environment, J. Appl. Meteorol., 30, 585–597, 1991.
Münkel, C. and Roininen, R.: Mixing layer height assessment with a compact lidar ceilometer, Symposium on Recent Developments in Atmospheric Applications of Radar and Lidar, New Orleans, LA, 20–25 January 2008, P2.2, 2008.
Münkel, C., Eresmaa, N., Rasanen, J., and Karppinen, A.: Retrieval of mixing height and dust concentration with lidar ceilometer, Bound.-Lay. Meteorol., 124, 117–128, 2007.
National Oceanic and Atmospheric Administration 2010 CalNex White Paper – Research at the Nexus of Air Quality and Climate Change: http://www.esrl.noaa.gov/csd/projects/calnex/whitepaper.pdf, last access: 7 July 2012, 2008.
National Research Council: Observing Weather and Climate from the Ground Up – A Nationwide Network of Networks, The National Academies Press, Washington, DC, 2009.
Neuman, J. A., Trainer, M., Aikin, K. C., Angevine, W. M., Brioude, J., Brown, S. S., de-Gouw, J. A., Dube, W. P., Flynn, J. H., Graus, M., Holloway, J. S., Lefer, B. L., Nedelec, P.,

ACPD
13, 13721–13772, 2013

Nowak, J. B., Parrish, D. D., Pollack, I. B., Roberts, J. M., Ryerson, T. B., Smit, H., Thouret, V., and Wagner, N. L.: Observations of ozone transport from the free troposphere to the Los Angeles basin, J. Geophys. Res.-Atmos., 117, D00V09, doi:10.1029/2011JD016919, 2012.

Noonkester, V. R., Jensen, D. R., Richter, J. H., Viezee, W., and Collis, R. T. H.: Concurrent FM-CW radar and lidar observations of the boundary layer, J. Appl. Meteorol., 13, 249–256, 1974.

Palm, S. P., Benedetti, A., and Spinhirne, J.: Validation of ECMWF global forecast model parameters using GLAS atmospheric channel measurements, Geophys. Res. Lett., 32, L22S09, doi:10.1029/2005GL023535, 2005.

Pottier, J. L., Pryor, S. C., and Banta, R. M.: Synoptic variability related to boundary layer and surface features observed during Pacific '93, Atmos. Environ., 31, 2163–2173, 1997.

Rogers, R. R., Hair, J. W., Hostetler, C. A., Ferrare, R. A., Obland, M. D., Cook, A. L., Harper, D. B., Burton, S. P., Shinozuka, Y., McNaughton, C. S., Clarke, A. D., Redemann, J., Russell, P. B., Livingston, J. M., and Kleinman, L. I.: NASA LaRC airborne high spectral resolution lidar aerosol measurements during MILAGRO: observations and validation, Atmos. Chem. Phys., 9, 4811–4826, doi:10.5194/acp-9-4811-2009, 2009.

Ryerson, T. B., Andrews, A. E., Angevine, W. M., Bates, T. S., Brock, C. A., Cairns, B., Cohen, R. C., Cooper, O. R., de Gouw, J. A., Fehsenfeld, F. C., Ferrare, R. A., Fischer, M. L., Flagan, R. C., Goldstein, A. H., Hair, J. W., Hardesty, R. M., Hostetler, C. A., Jimenez, J. L., Langford, A. O., McCauley, E., McKeen, S. A., Molina, L. T., Nenes, A., Oltmans, S. J., Parrish, D. D., Pierce, R. B., Prather, K., Quinn, P. K., Seinfeld, J. H., Senff, C. J., Sorooshian, A., Stutz, J., Surratt, J. D., Trainer, M., Volkamer, R., Williams, E. J., and Wofsy, S. C.: The 2010 California research at the Nexus of Air Quality and Climate Change (CalNex) field study, J. Geophys. Res.-Atmos., doi:10.1002/jgrd.50331, in press, 2013.

Schmid, P. and Niyogi, D.: A method for estimating planetary boundary layer heights and its application over the ARM southern great plains site, J. Atmos. Ocean Tech., 29, 316–322, 2012.

Seibert, P., Beyrich, F., Gryning, S. E., Joffre, S., Rasmussen, A., and Tercier, P.: Review and intercomparison of operational methods for the determination of the mixing height, Atmos. Environ., 34, 1001–1027, 2000.

Seidel, D. J., Ao, C. O., and Li, K.: Estimating climatological planetary boundary layer heights from radiosonde observations: comparison of methods and uncertainty analysis, J. Geophys. Res.-Atmos., 115, D16113, doi:10.1029/2009JD013680, 2010.

ACPD
13, 13721–13772, 2013

Stull, R. B.: An Introduction to Boundary Layer Meteorology. Atmospheric Sciences Library, Kluwer Academic Publisher, Dordrecht-Boston-London, 666 pp., 1988.

Wakimoto, R. and McElory, J.: Lidar observations of elevated pollution layers over Los Angeles, J. Clim. Appl. Meteorol., 25, 1583–1599, 1986.

Zaveri, R. A., Shaw, W. J., Cziczo, D. J., Schmid, B., Ferrare, R. A., Alexander, M. L., Alexandrov, M., Alvarez, R. J., Arnott, W. P., Atkinson, D. B., Baidar, S., Banta, R. M., Barnard, J. C., Beranek, J., Berg, L. K., Brechtel, F., Brewer, W. A., Cahill, J. F., Cairns, B., Cappa, C. D., Chand, D., China, S., Comstock, J. M., Dubey, M. K., Easter, R. C., Erickson, M. H., Fast, J. D., Floerchinger, C., Flowers, B. A., Fortner, E., Gaffney, J. S., Gilles, M. K., Gorkowski, K., Gustafson, W. I., Gyawali, M., Hair, J., Hardesty, R. M., Harworth, J. W., Herndon, S., Hiranuma, N., Hostetler, C., Hubbe, J. M., Jayne, J. T., Jeong, H., Jobson, B. T., Kassianov, E. I., Kleinman, L. I., Kluzek, C., Knighton, B., Kolesar, K. R., Kuang, C., Kubátová, A., Langford, A. O., Laskin, A., Laulainen, N., Marchbanks, R. D., Mazzoleni, C., Mei, F., Moffet, R. C., Nelson, D., Obland, M. D., Oetjen, H., Onasch, T. B., Ortega, I., Ottaviani, M., Pekour, M., Prather, K. A., Radney, J. G., Rogers, R. R., Sandberg, S. P., Sedlacek, A., Senff, C. J., Senum, G., Setyan, A., Shilling, J. E., Shrivastava, M., Song, C., Springston, S. R., Subramanian, R., Suski, K., Tomlinson, J., Volkamer, R., Wallace, H. W., Wang, J., Weickmann, A. M., Worsnop, D. R., Yu, X.-Y., Zelenyuk, A., and Zhang, Q.: Overview of the 2010 Carbonaceous Aerosols and Radiative Effects Study (CARES), Atmos. Chem. Phys., 12, 7647–7687, doi:10.5194/acp-12-7647-2012, 2012.

ACPD
13, 13721–13772, 2013

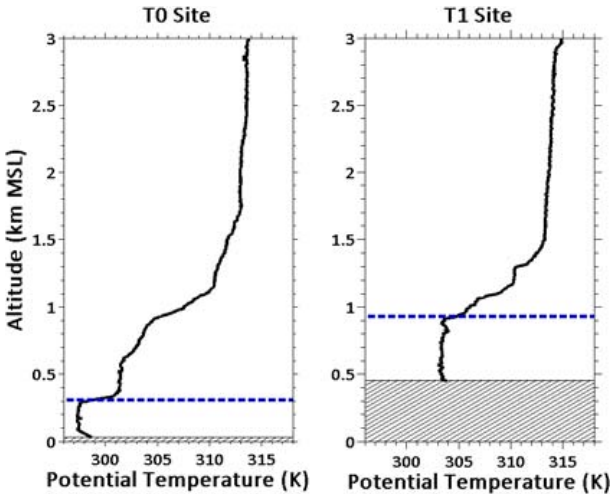

Fig. 1. Potential temperature profiles from radiosondes launched at the T0 and T1 sites during the CARES campaign on 27 June 2010 at 17:00 UTC. The PBL height (blue dashed line) at the T0 site is 0.31 km and the height at the T1 site is 0.93 km.

ACPD
13, 13721–13772, 2013

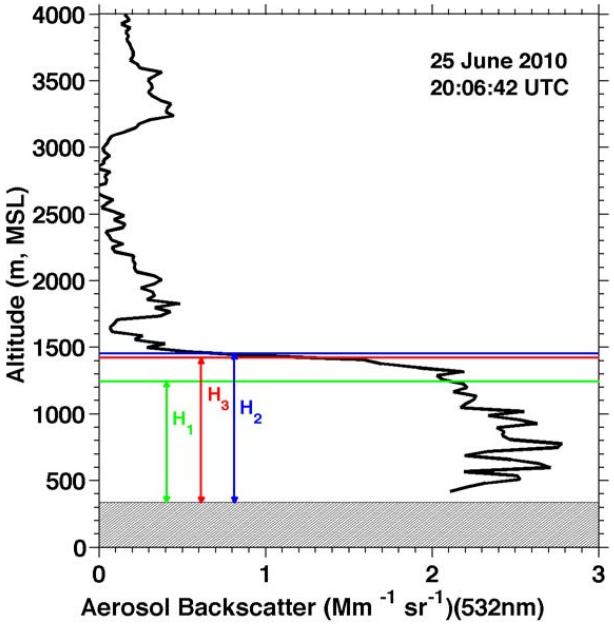

Fig. 2. HSRL backscatter profile acquired at 20:06:42 UTC on 25 May 2010. The ML heights H_1, H_2, and H_3, which are derived from the modified Brooks algorithm, are shown.

ACPD
13, 13721–13772, 2013

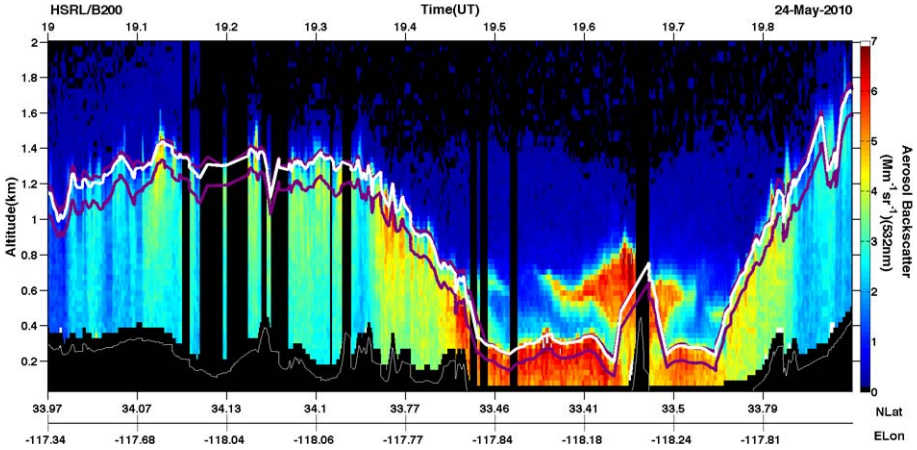

Fig. 3. HSRL backscatter profiles on 24 May 2010. Deep purple lines show one-minute average bottom (H_1) and top (H_2) transition zone heights, and the white line shows the one-minute average height of the maximum in the wavelet transform of the Haar function.

ACPD
13, 13721–13772, 2013

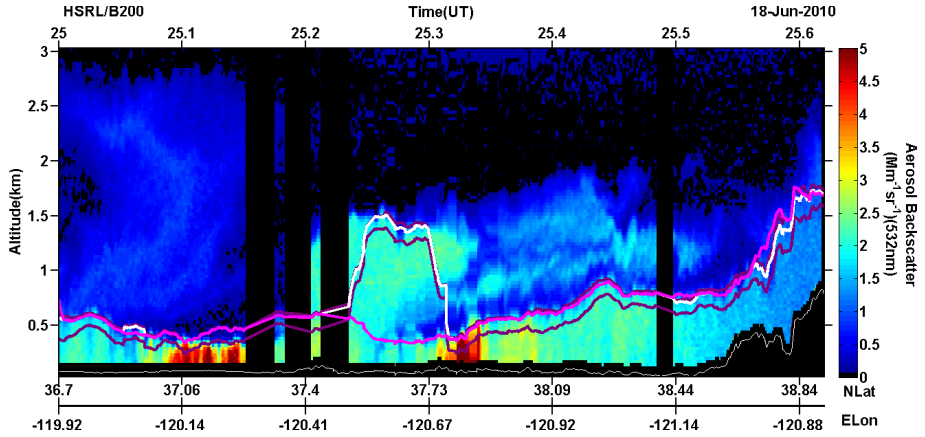

Fig. 4. Same as Fig. 3 except for 18 June 2010. The magenta line shows the "best estimate" ML height.

ACPD
13, 13721–13772, 2013

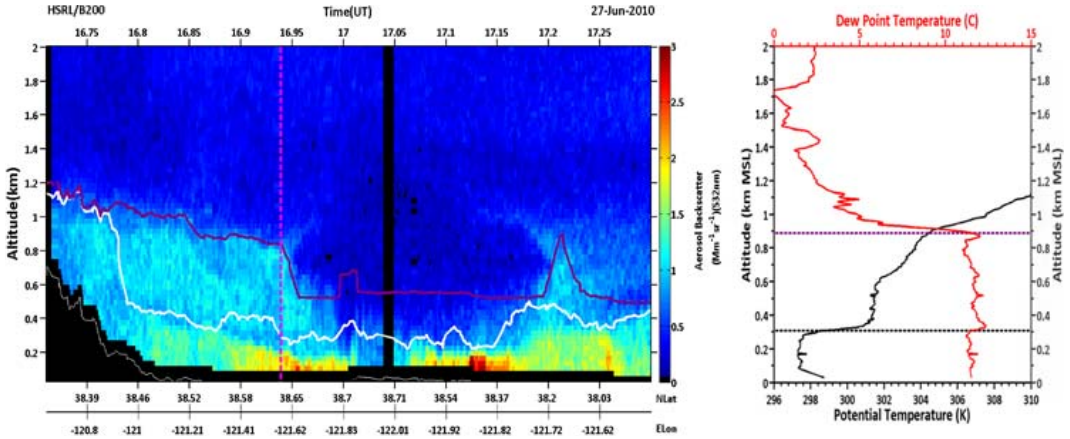

Fig. 5. (left) HSRL aerosol backscatter profiles on 27 June 2010 with the ML height (white line) and maximum aerosol gradient (purple line) matches the height corresponding to gradients (PBL height is black dashed line) in the (right) radiosonde profile of potential temperature and dew point measured just before 17:00 UTC on this day (corresponding to the magenta dashed line in the lidar image.)

ACPD
13, 13721–13772, 2013

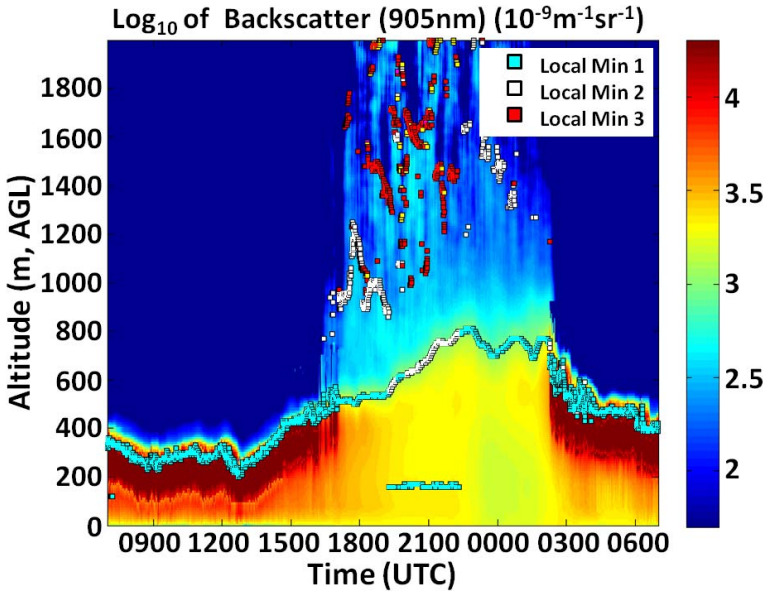

Fig. 6. Log_{10} of the aerosol backscatter on 16–17 May 2010 using ceilometer retrievals from the CalNex Pasadena, CA ground site. Three gradient local minima (Local Min) are indicated by the colored squares. The Local Min values are used in the ML height comparisons found in Sect. 4.1.

ACPD
13, 13721–13772, 2013

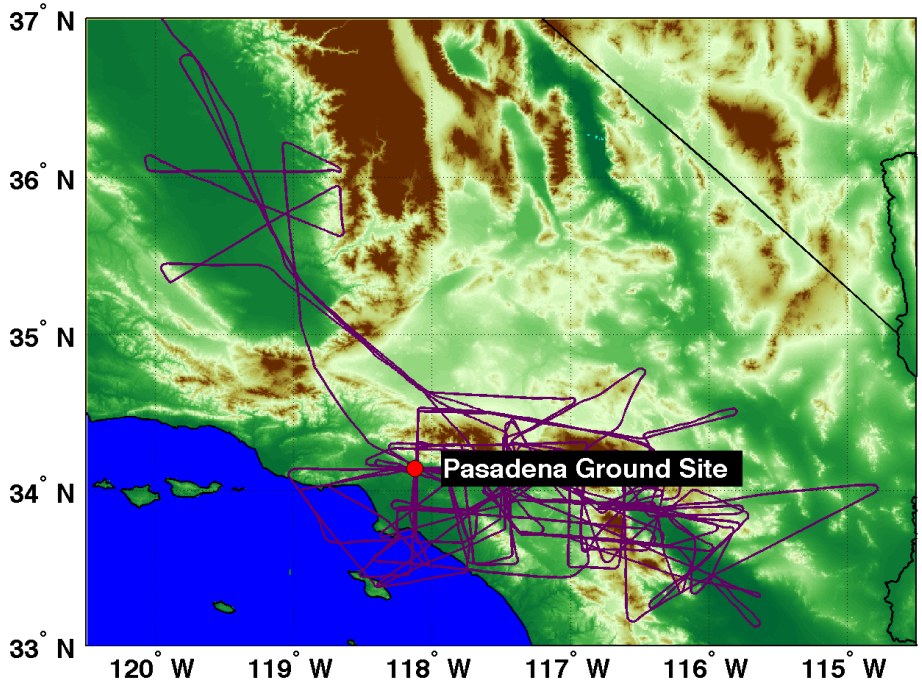

Fig. 7. Summary of flight tracks during CalNex and the location of the ground site in Pasadena, CA.

ACPD
13, 13721–13772, 2013

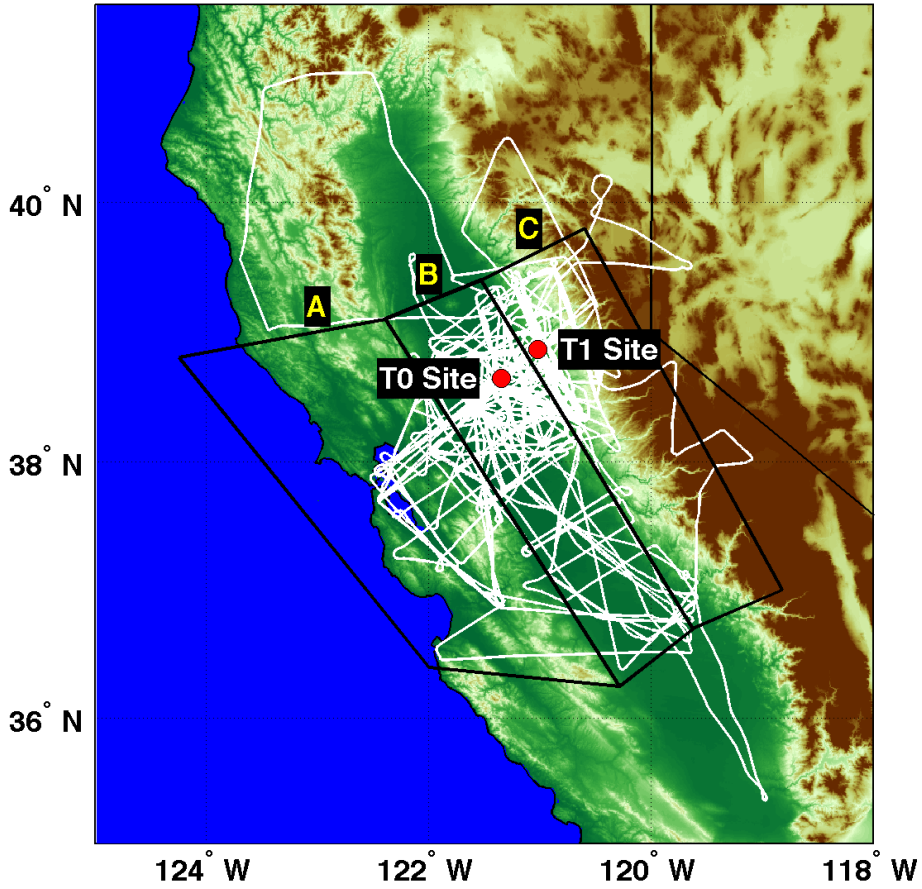

Fig. 8. Summary of flight tracks during CARES along with the three study regions (A. San Francisco, B. Central Valley and C. Sierra Nevada) discussed in Sect. 4.2.2 and locations of the two ground sites.

ACPD
13, 13721–13772, 2013

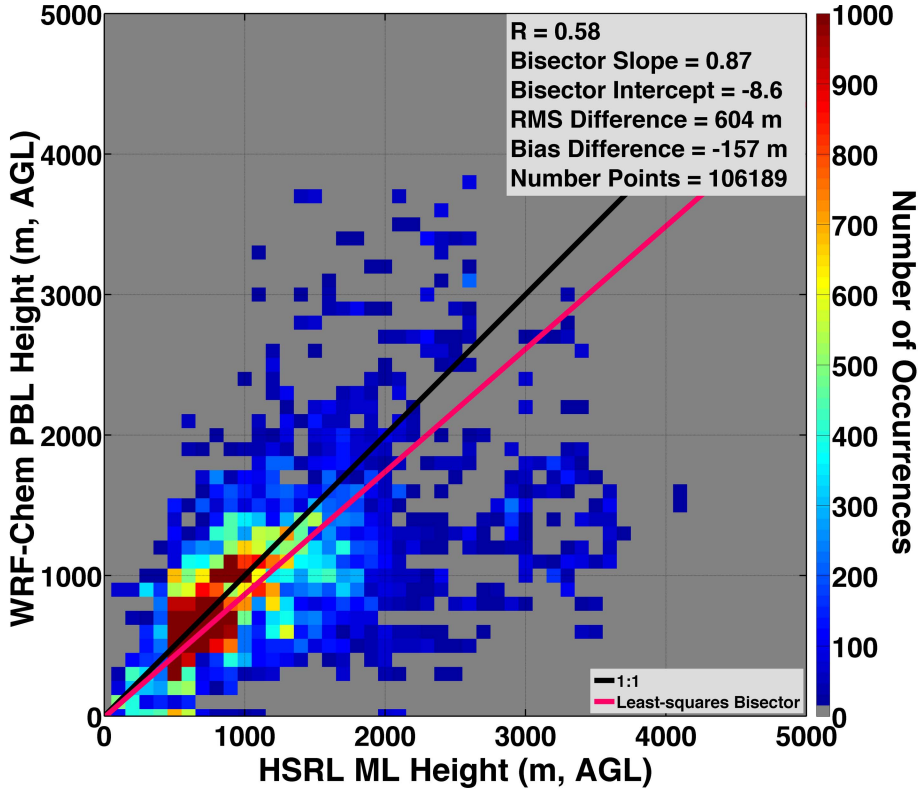

Fig. 9. Scatter and regression plot of WRF-Chem PBL and HSRL ML heights across all flights during CalNex. Number of occurrences in each histogram bin is shown in color. Bias and RMS Difference calculated WRF-Chem – HSRL.

ACPD
13, 13721–13772, 2013

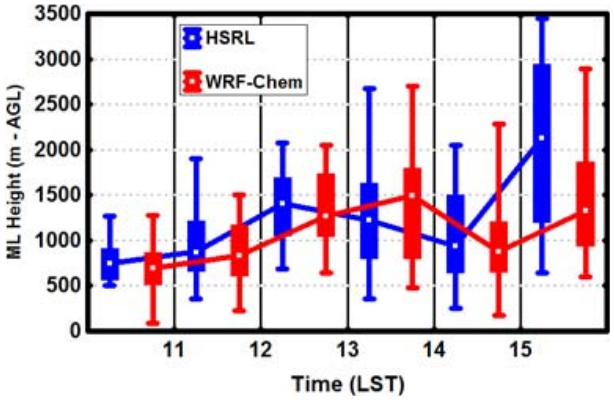

Fig. 10. Diurnal variation for HSRL ML heights and WRF-Chem PBL heights over the entire campaign. Filled boxes denote the 25th and 75th percentiles and vertical lines denote the 5th and 95th percentiles. Lines connecting the white dots denote the median value for each hour. The blue and red boxes are gridded by time and offset for clarity (e.g. the first HSRL (blue) and WRF-Chem (red) boxes represent the heights from 10:00–11:00 LST).

ACPD
13, 13721–13772, 2013

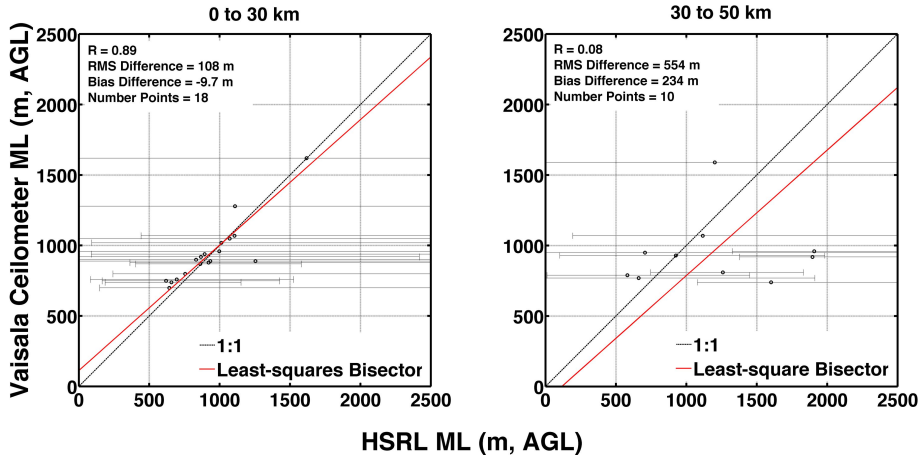

Fig. 11. Scatter and regression plots of HSRL and ceilometer ML heights as a function of distance of closest approach of the aircraft to the ceilometer. The circles compare the ceilometer measurement to the HSRL data taken at the point of closest approach to the Pasadena ground site. The horizontal lines indicate the spread of all HSRL-derived ML heights encountered as the B-200 flew within ±7.5 min of each ceilometer measurement, though not limited by separation distance and give an indication of spatial variability of the ML height.

ACPD
13, 13721–13772, 2013

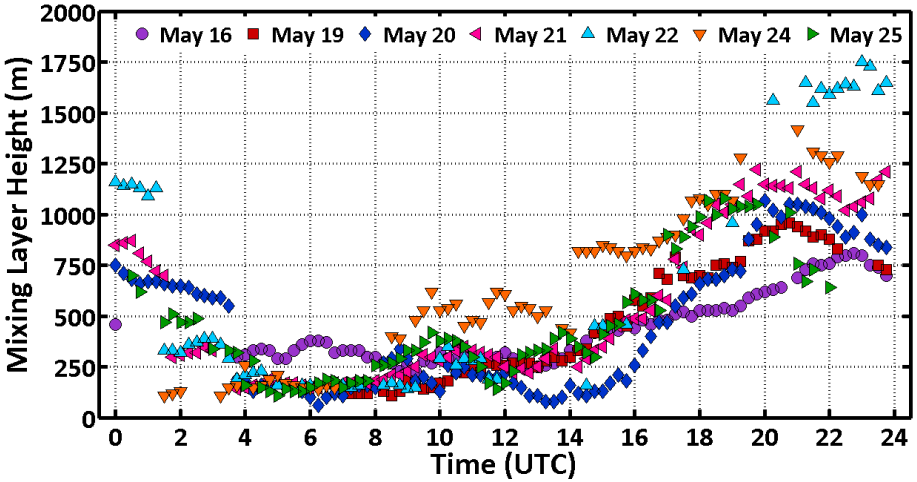

Fig. 12. Diurnal pattern of the ceilometer ML heights when HSRL and ceilometer data were available.

ACPD
13, 13721–13772, 2013

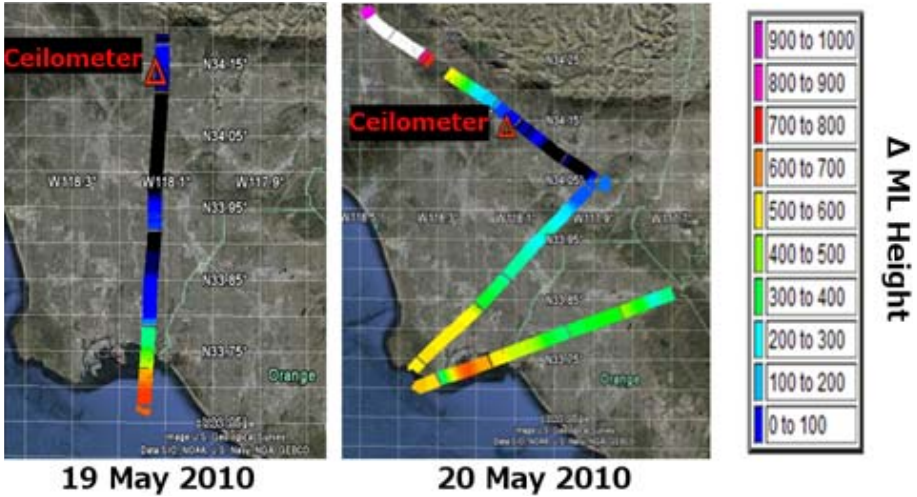

Fig. 13. Google Earth images displaying the differences between the HSRL and ceilometer ML heights in meters for portions of two flights during CalNex (ΔML Height = HSRL – ceilometer). Data on 19 May were taken from about 21:00 UTC (14:00 LST) to 21:10 UTC (14:10 LST). Data on 20 May were taken from about 19:45 UTC (12:45 LST) to 20:15 UTC (13:15 LST).

ACPD
13, 13721–13772, 2013

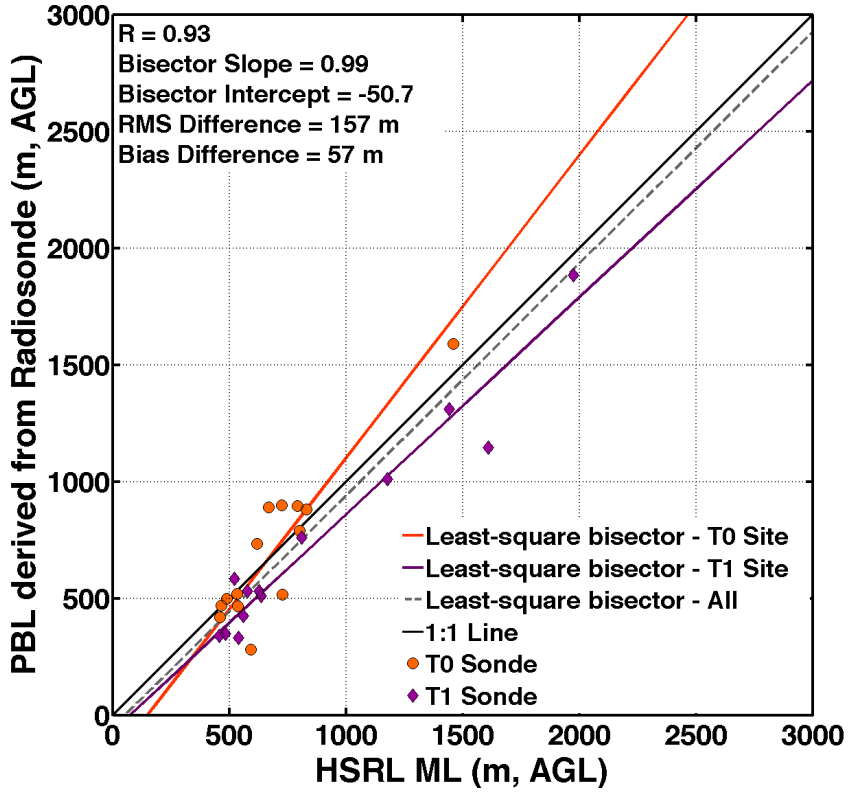

Fig. 14. Scatter and regression plot of HSRL ML heights and radiosonde PBL heights within 15 km and 30 min. of the ground sites. The statistics in the upper left corner are for the comparisons when both the T0 and T1 sites are combined.

ACPD
13, 13721–13772, 2013

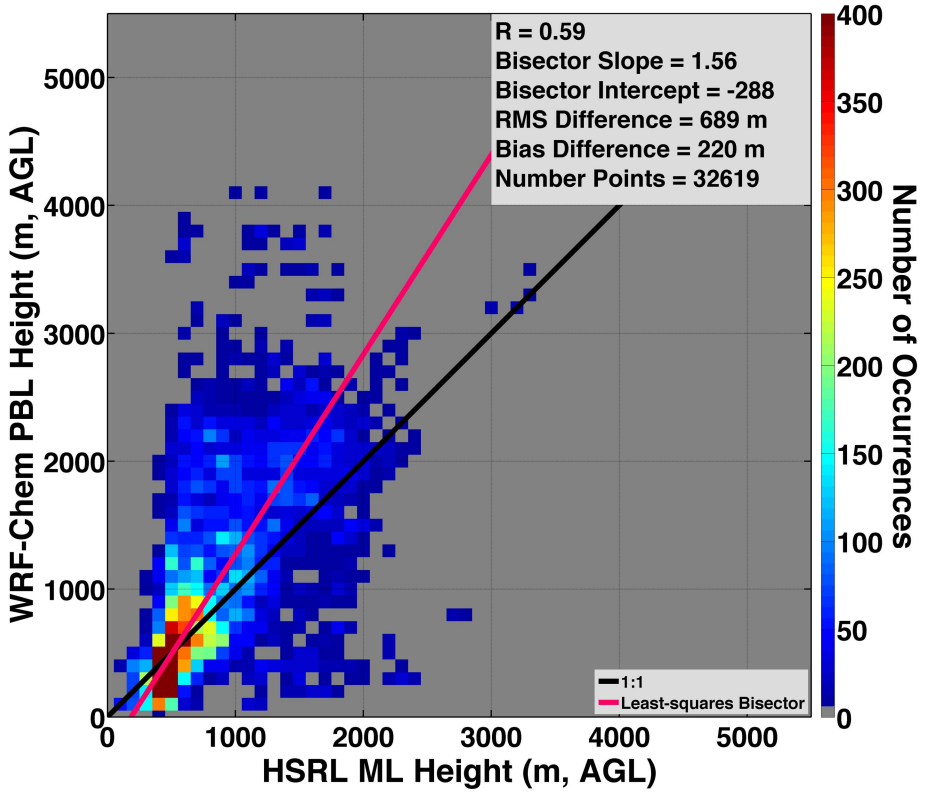

Fig. 15. Scatter and regression plot of WRF-Chem PBL and HSRL ML heights across all flights during CARES. The PBL heights for WRF-Chem are derived from potential temperature. Number of occurrences in each histogram bin is shown in color. Bias and RMS Difference calculated WRF-Chem – HSRL.

ACPD
13, 13721–13772, 2013

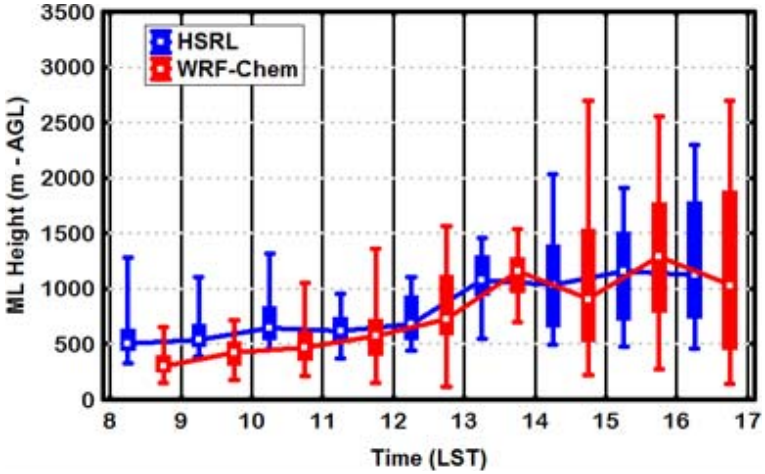

Fig. 16. Diurnal variation for HSRL ML heights and WRF-Chem PBL heights over the entire CARES campaign. Filled boxes denote the 25th and 75th percentiles and vertical lines denote the 5th and 95th percentiles. Lines connecting the white dots denote the median value for each hour. The blue and red boxes are gridded by time and offset for clarity (e.g. the first HSRL (blue) and WRF-Chem (red) boxes represent the heights from 08:00–09:00 LST).

ACPD
13, 13721–13772, 2013

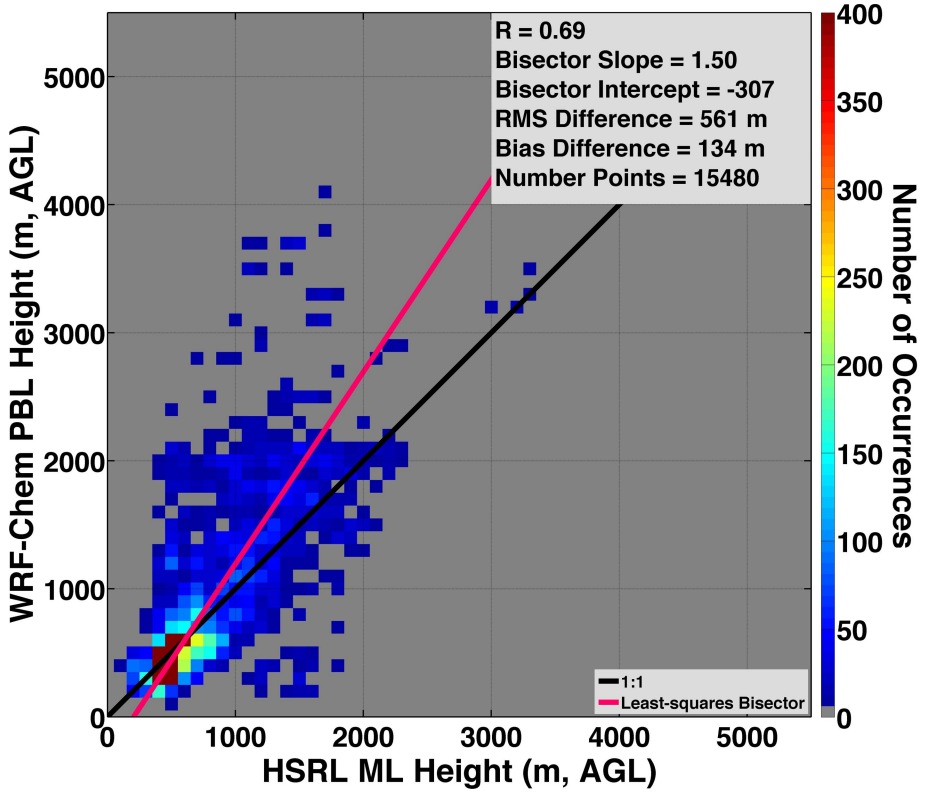

Fig. 17. Scatter and regression plot of WRF-Chem PBL and HSRL ML heights during CARES for the flights within the Central Valley region. Number of occurrences in each histogram bin is shown in color. Bias and RMS Difference calculated WRF-Chem – HSRL.

ACPD
13, 13721–13772, 2013

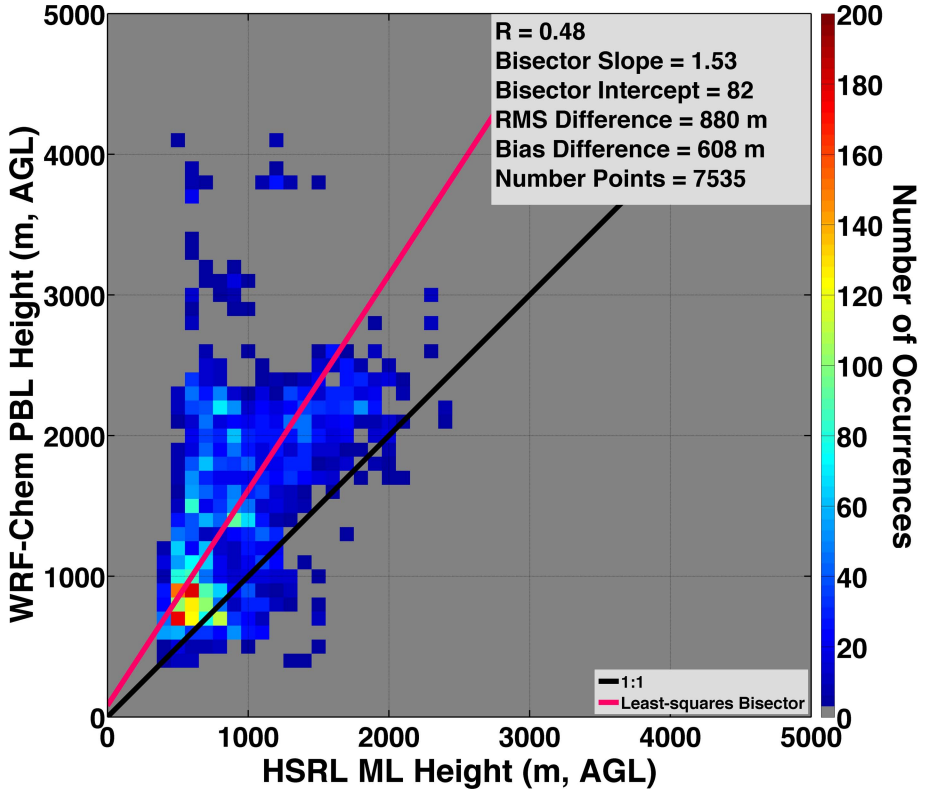

Fig. 18. Scatter and regression plot of WRF-Chem PBL and HSRL ML heights during CARES for the flights within the Sierra Nevada region. Number of occurrences in each histogram bin is shown in color. Bias and RMS Difference calculated WRF-Chem – HSRL.

ACPD
13, 13721–13772, 2013

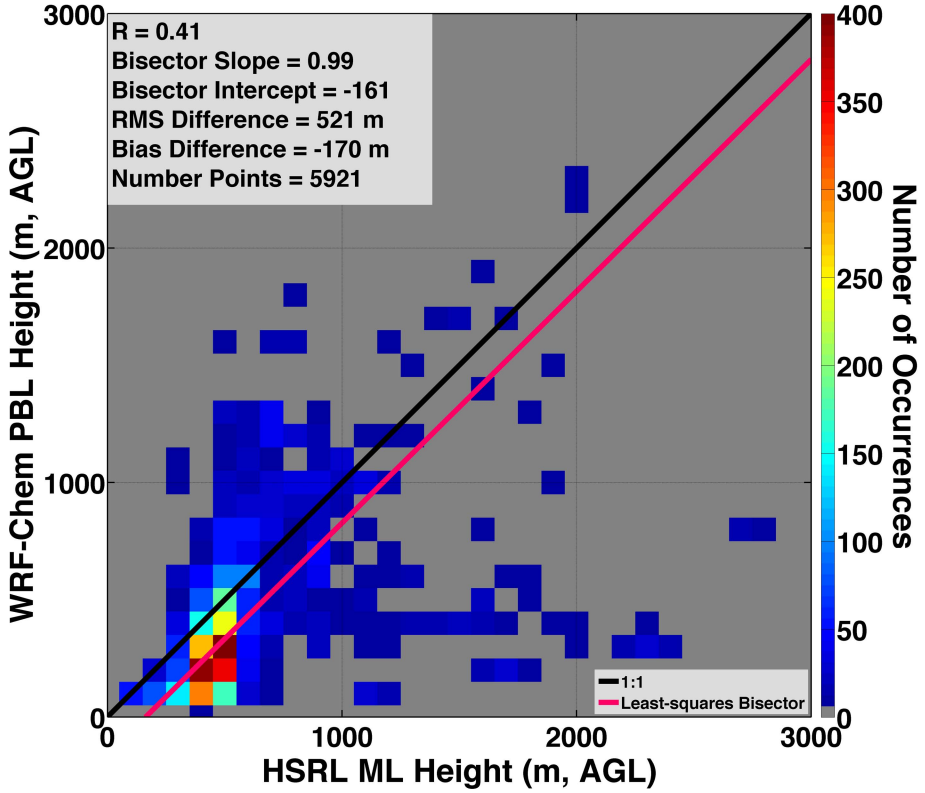

Fig. 19. Scatter and regression plot of WRF-Chem PBL and HSRL ML heights during CARES for the flights within the San Francisco Bay region. Number of occurrences in each histogram bin is shown in color. Bias and RMS Difference calculated WRF-Chem – HSRL.

ACPD
13, 13721–13772, 2013

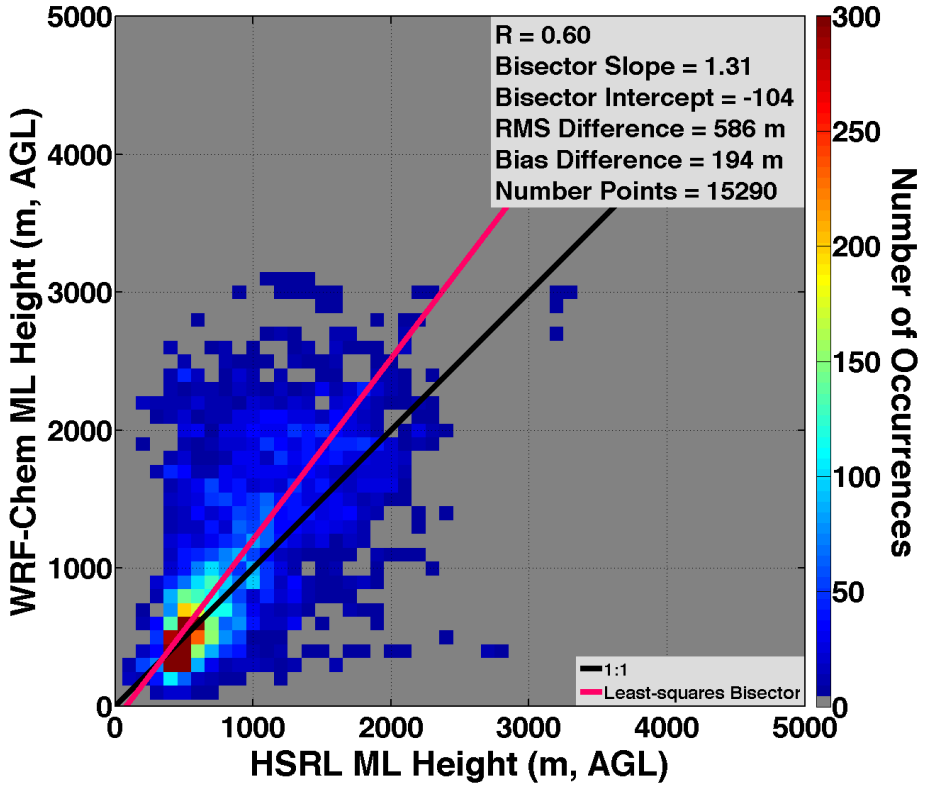

Fig. 20. Scatter and regression plot of WRF-Chem and HSRL ML heights across all flights during CARES. This plot is similar to Fig. 15, except that the WRF-Chem ML heights are derived from the simulated aerosol backscatter. Number of occurrences in each histogram bin is shown in color. Bias and RMS Difference calculated WRF-Chem – HSRL.

ACPD
13, 13721–13772, 2013

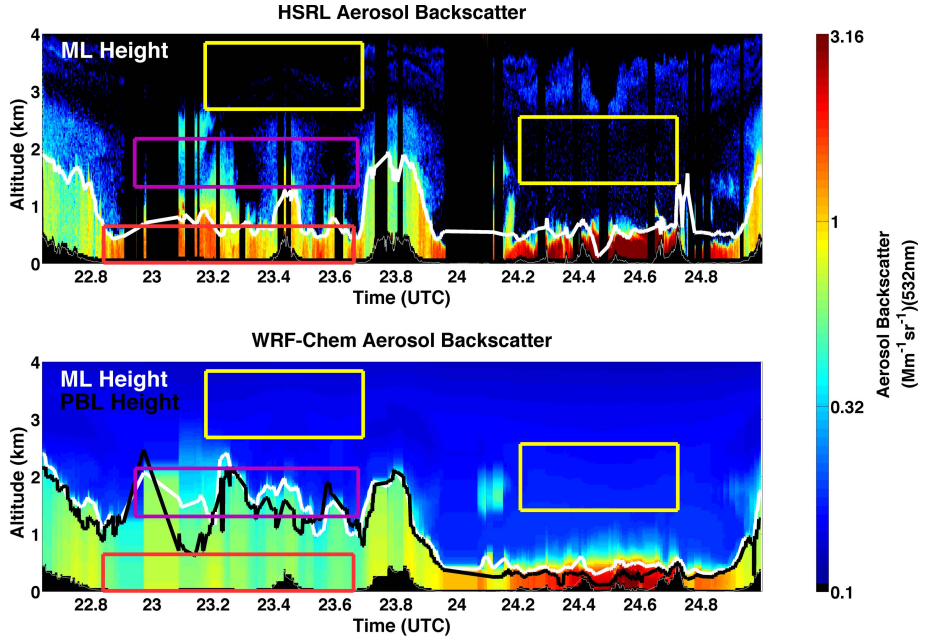

Fig. 21. (Top) Aerosol backscatter measured from HSRL with ML heights derived from aerosol backscatter and (Bottom) simulated aerosol backscatter from WRF-Chem with PBL heights derived from potential temperature (in black) and ML heights derived from aerosol backscatter (in white); data are from the second research flight on 14 June 2010. The colored boxes refer to regions that are discussed in Fig. 22.

ACPD
13, 13721–13772, 2013

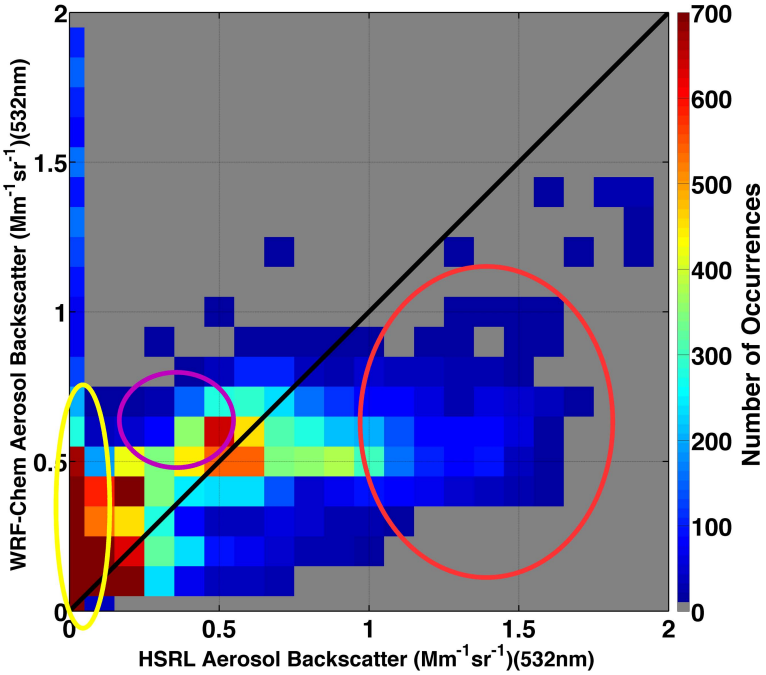

Fig. 22. Scatter density plot of observed HSRL and simulated WRF-Chem backscatter for the second flight on 14 June 2010. The area circled in yellow indicates the WRF-Chem values are high in the free troposphere. The area circled in purple is where the WRF-Chem simulations had difficulty forecasting the vertical extent of aerosols in the ML, over predicted the height of the PBL, and where the simulated backscatter concentration is higher due to the higher vertical extent of the simulated PBL. The area circled in red demonstrates where the HSRL aerosol backscatter is more concentrated within the ML (e.g. between 22.8 and 23.6 UTC in Fig. 21). The colored circles correspond to the colored boxes in the backscatter plot in Fig. 21.

ACPD
13, 13721–13772, 2013